Zero Thermal Expansion Effect and Enhanced Magnetocaloric Effect Induced by Fe Vacancies in $Fe_2Hf_{0.80}Nb_{0.20}$ Laves Phase Alloys

Shen, Qi; Zhang, Zeyu; de Vries, Calvin; Dugulan, Achim Iulian; van Dijk, Niels; Brück, Ekkes; Li, Lingwei

DOI
10.1021/acs.chemmater.4c01345

Publication date
2024

Document Version
Final published version

Published in
Chemistry of Materials

CHEMISTRY OF MATERIALS

pubs.acs.org/cm

Article

Zero Thermal Expansion Effect and Enhanced Magnetocaloric Effect Induced by Fe Vacancies in $Fe_2Hf_{0.80}Nb_{0.20}$ Laves Phase Alloys

Qi Shen, Zeyu Zhang, Calvin de Vries, Achim Iulian Dugulan, Niels van Dijk, Ekkes Brück, and Lingwei Li*

Cite This: *Chem. Mater.* 2024, 36, 6299−6305

Read Online

ACCESS | Metrics & More | Article Recommendations | Supporting Information

ABSTRACT: Zero thermal expansion (ZTE) materials with the advantage of an invariable length with varying temperatures are in high demand for modern industry but are relatively rare for metals. Fe-based Laves phases attract significant attention due to the rich and intriguing physical properties resulting from the coupling between crystal, electric, and magnetic structures. In this work, the structural, magnetic transition, thermal expansion, and magnetocaloric effect of single-phase $Fe_{2-x}Hf_{0.80}Nb_{0.20}$ Laves phase alloys were investigated by means of macroscopic magnetic measurements, Mössbauer spectroscopy, and X-ray diffraction at the temperature range of 4.2−400 K. With the introduction of Fe vacancies, the ZTE coefficient of −1.2 ppm/K is smaller than that (1.7 ppm/K) of stoichiometric $Fe_2Hf_{0.80}Nb_{0.20}$ alloy. Meanwhile, the magnetic entropy change experiences an enhancement from 0.39 to 0.50 J/kg K at a magnetic field change of 2 T. These improved properties are attributed to the vacancy-induced coexistence of ferromagnetic and antiferromagnetic phases, as evidenced by variable-temperature X-ray diffraction and Mössbauer spectroscopy. This work unveils a promising avenue for new zero thermal expansion materials by controlling the vacancies at magnetic atom positions in Fe-based Laves phase alloys.

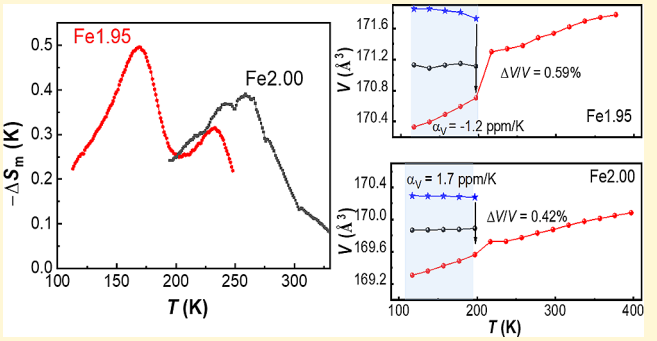

INTRODUCTION

The hexagonal C14 structure Fe-based Laves phases stand out within the Laves phase family due to their remarkable sensitivity of crystal, magnetism, and electronic properties to compositional variations.[1−5] Among them, Fe_2(Hf,Ta) alloys have garnered considerable attention due to the itinerant-electron metamagnetic transition from ferromagnetic (FM) to antiferromagnetic (AFM) state as the temperature increases.[4,6−8] This FM−AFM transition is attributed to a frustration effect, where the ordered magnetic moment of the Fe atom at the 2a site, situated within the middle layer of the Fe atom at the 6h site, vanishes as the temperature exceeds the transition temperature.[9−11] A significant research interest has been attracted in Fe-based Laves phase alloys including the mechanism underlying this metamagnetic transition[7,11−14] and related rich physical properties such as magnetocaloric effect,[15−17] negative thermal expansion (NTE) or zero thermal expansion (ZTE),[7,18−20] and magnetoresistance.[14] A large adiabatic temperature change (3.5 K) from the metamagnetic transition was obtained at a magnetic field change of 2 T,[16] which is comparable to the values for the two well-known MCE materials $La(Fe_{0.88}Si_{0.12})_{13}H_y$[21] and $Mn_xFe_{2-x}P_{1-y}Si_y$.[22] Accompanied by the FM−AFM transition, a NTE coefficient as large as −16.3 ppm/K is observed in $Fe_2Hf_{0.87}Ta_{0.13}$ over a broad temperature window of 222−327 K.[7] Therefore, the magnetoelastic transition in the Fe-based Laves phase makes them attractive for thermal expansion and magnetocaloric applications.

In recent studies, pseudobinary Fe_2(Hf, Nb) alloys have also emerged as exhibiting a FM−AFM transition accompanied by a negative/zero thermal expansion.[2,23,24] The magnetic phase diagram presented by Yibole et al.[2] delineates this transition within the range of x = 0.17−0.26. It is worthwhile to note that the AFM−FM transition in Fe_2(Hf,Nb) alloys exhibits a broader profile compared to that of Fe_2(Hf,Ta) alloys, which can be attributed to the coexistence of AFM and FM phases below the transition temperature. A similar negative volume thermal expansion of $\alpha_V = -9.26 \times 10^{-6}$ K^{-1} is observed in the $Fe_2Hf_{0.85}Nb_{0.15}$ alloy in the temperature range of 130−300 K.[23] Modulating the magnetic interactions by tuning the non-stoichiometric chemical composition can be an effective approach to achieve ZTE in magnetic materials, as reported in the $Fe_{2.5}Hf$ Laves phase (1.25 ppm/K, 433−583 K) by

Received: May 9, 2024
Revised: June 4, 2024
Accepted: June 5, 2024
Published: June 12, 2024

adding excess Fe[25] and in $Mn_3Zn_{0.96}N$ (−4.11 ppm/K, 125−185 K) by introducing Zn vacancies.[26] In this work, we explore the impact of Fe content on the structure, magnetic transition, thermal expansion, and magnetocaloric effect in the $Fe_2Hf_{0.80}Nb_{0.20}$ (x = −0.05, 0, 0.05) system by variable-temperature X-ray diffraction and Mössbauer spectroscopy. We found enhanced MCE and ZTE effects in the $Fe_{1.95}Hf_{0.80}Nb_{0.20}$ composition, offering a novel perspective on designing ZTE materials by manipulating vacancies within magnetic atoms in Fe-based Laves phase alloys.

EXPERIMENTAL SECTION

Polycrystalline $Fe_{2-x}Hf_{0.80}Nb_{0.20}$ (x = −0.05, 0, and 0.05) alloys were prepared from high-purity elements (Fe 99.98%, Hf 99.95%, and Ti 99.99%) by arc melting. For ease of reference, the samples corresponding to x = −0.05, 0, and 0.05 are denoted as Fe1.95, Fe2.00, and Fe2.05 alloys, respectively. Samples with a total mass of 5 g were melted four or five times, and the button-shaped alloys were flipped over after each melting. The weight loss was confirmed to be less than 0.5% after each arc-melting process. To suppress phase segregation, the power supply was promptly deactivated after each arc melting cycle. As heat treatments yielded negligible improvements in the magnetic properties for Fe_2(Hf,Nb),[2] the arc-melted samples in this study were not subjected to any annealing processes.

X-ray diffraction (XRD) data were acquired using a PANalytical X-Pert PRO system with Cu-K_α radiation and an Anton Paar TTK 450 temperature chamber. The lattice structure was analyzed through Rietveld refinement employing Fullprof.[27] The magnetic properties at low temperature (4−370 K) were measured using a superconducting quantum interference device (SQUID) magnetometer model MPMS-XL, equipped with the reciprocating sample option. The ferromagnetic transition temperature T_C is determined from the minimum in the temperature derivative magnetization as a function of temperature at an applied magnetic field of 0.1 T. The magnetic entropy change was calculated from the $M-T$ curves obtained at different magnetic fields by using the Maxwell relations. The microstructure was analyzed by scanning electron microscopy (SEM) using a FEI Quanta FEG 450 equipped with energy-dispersive X-ray spectroscopy (EDS). Transmission ^{57}Fe Mössbauer spectra were collected at different temperatures with conventional constant-acceleration or sinusoidal-velocity spectrometers using a ^{57}Co(Rh) source. The velocity calibration was performed using an α-Fe foil at room temperature. The source and absorbing samples were kept at the same temperature during the cryogenic measurements. The Mössbauer spectra were subsequently fitted using the Mosswinn 4.0 program.[28]

RESULTS AND DISCUSSION

Figure 1a displays the XRD patterns of the Fe1.95, Fe2.00, and Fe2.05 alloys at room temperature, exhibiting crystallization in a single hexagonal $MgZn_2$ Laves phase structure (space group: $P6_3/mmc$). Figure 1b displays the refined XRD pattern of the Fe1.95 alloy based on the crystal structure of $MgZn_2$ depicted in Figure 1c. The unit-cell volume of the Fe1.95, Fe2.00, and Fe2.05 alloys is 170.50, 170.33, and 170.19 Å^3, respectively. This trend is consistent with the observations of $Fe_{2+x}Hf_{0.82}Nb_{0.18}$ (x = −0.05 to 0.09)[2] and $Fe_{2+x}Hf_{0.83}Ta_{0.17}$ (x = −0.18 to 0.26),[29] which indicate that excess Fe atoms may substitutionally occupy the (Hf/Ta) 4f site. Notably, even in stoichiometric Fe_2(Hf,Ta) compounds, Fe atoms show a preference for the 4f site, as evidenced by the pronounced magnetization change in slightly Fe-deficient Fe_2(Hf,Ta) alloys.[29,30] Unlike the as-cast $Fe_2Hf_{0.80}Nb_{0.20}$ alloy in ref 2, which exhibited a Nb-/Hf-rich secondary phase at grain boundaries, the SEM image and line-scan profile along the yellow line in Figure 1d confirm the microstructural homogeneity of the single-phase Fe1.95 alloy at a 30 μm length scale. In this study, the immediate deactivation of the power switch likely mitigated the tendency for Nb and Hf atom segregation, since the rapid solidification process can suppress phase segregation, as observed in the melt-spun $Fe_2Hf_{0.85}Ti_{0.15}$ alloy.[12]

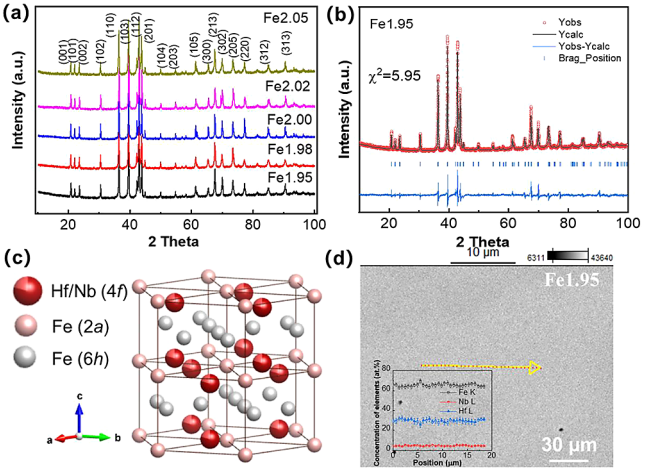

Figure 1. (a) XRD patterns of the Fe1.95, Fe2.00, and Fe2.05 alloys, with peaks indexed by the $MgZn_2$-type structure. The lattice parameters are a = 4.937 Å, c = 8.077 Å for the Fe1.95 alloy, a = 4.936 Å, c = 8.072 Å for the Fe2.00 alloy, and a = 4.935 Å, c = 8.068 Å for the Fe2.05 alloy. (b) Refined XRD patterns of the Fe1.95 alloy. (c) Crystal structure of the $MgZn_2$-type structure for the $Fe_{2-x}Hf_{0.80}Nb_{0.20}$ Laves phase. (d) Backscattered electron image of the Fe1.95 alloy and a line-scan profile along the yellow line in the image.

Figure 2a shows the $M-T$ curves at a magnetic field of 0.1 T for the Fe1.95, Fe2.00, and Fe2.05 alloys. The thermal hysteresis of 1−2 K observed in the $M-T$ curves for all three alloys indicates a first-order magnetic transition. The higher magnetization observed in the Fe2.05 alloy can be attributed to the substitution of extra Fe for Hf/Nb atoms at the 4f sites, as evidenced by its smaller unit-cell volume compared to those of the Fe1.95 and Fe2.00 alloys. A magnetization bump observed at 153 K for the Fe1.95 alloy suggests a two-step magnetic transition. Annealing at 1273 K for 24 h does not alert the two-step magnetization change behavior, as shown in Figure S1 in the Supporting Information. For the Fe1.95 and the Fe2.00 alloys, the FM−AFM transition temperatures (T_t) are 225 and 253 K, respectively. A kink at 340 K for the Fe1.95 alloy corresponds to the AFM−PM transition temperature (T_N). The T_t and T_N values for the Fe1.95 and Fe2.00 alloys are consistent with the magnetic phase diagram given in ref 2. The $M-H$ curves in Figure 2c show the magnetic hysteresis observed in these three alloys. The saturation magnetization of the Fe1.95 alloy is 47 A m^2/kg, representing an 11% increase compared to that of the Fe2.00 alloy (43 A m^2/kg). An additional near-linear contribution to the magnetization in Figure 2b and a substantial reduction in magnetic hysteresis after one cycle in Figure S2 in the Supporting Information are observed for the Fe1.95 alloy, in accordance with the results for the Fe_2(Hf,Nb) alloys reported in ref 2. The application of an external magnetic field can partially induce the conversion of the AFM into the FM phase, which contributes to the enhanced saturation magnetization of the Fe1.95 alloy.[31] These results indicate an incomplete AFM−FM transition occurring below T_t, resulting in the coexistence of the AFM phase and the FM phase at 5 K.

https://doi.org/10.1021/acs.chemmater.4c01345
Chem. Mater. 2024, 36, 6299−6305

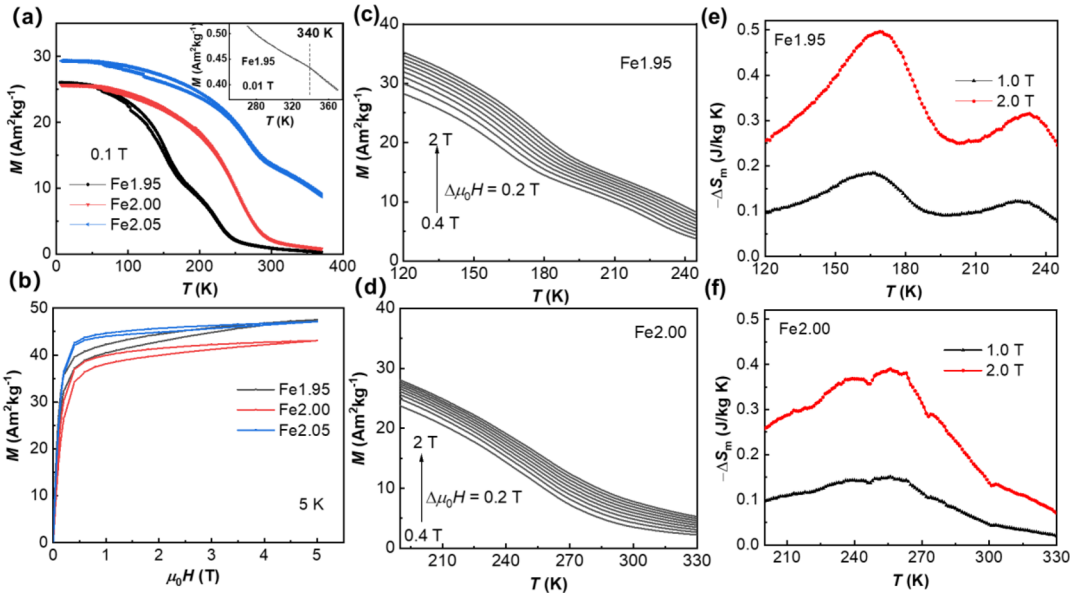

Figure 2. (a) $M-T$ curves for the Fe1.95, Fe2.00, and Fe2.05 alloys in a magnetic field of 0.1 T. The inset shows the details in the vicinity of T_N in a magnetic field of 0.01 T. (b) $M-H$ curves for the Fe1.95, Fe2.00, and Fe2.05 alloys at a temperature of 5 K. $M-T$ curves upon heating at different applied magnetic fields for (c) the Fe1.95 alloy and (d) the Fe2.00 alloy. $|\Delta S_m|$ calculated from the heating curves for (e) the Fe1.95 alloy and (f) the Fe2.00 alloy.

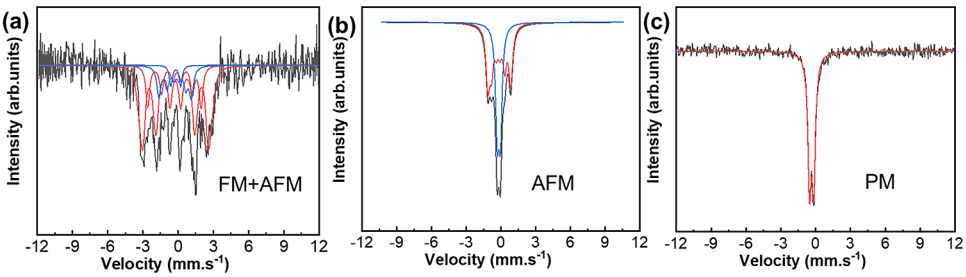

Figure 3. Mössbauer spectra for the Fe1.95 alloy at (a) 4.2, (b) 300, and (c) 400 K.

Table 1. Mössbauer Fitted Parameters of the Fe1.95 Alloy at Different Temperatures[a]

sample	T (K)	IS (mm s^{-1})	QS (mm s^{-1})	hyperfine field (T)	Γ (mm s^{-1})	phase
arc-melted Nb0.20	4.2 K	−0.23	0.01	18.0	0.40	59.7% (FM-6h)
		−0.21	−0.11	14.1	0.37	19.9% (FM-2a)
		−0.21	−0.10	14.1	0.37	16.4% (AFM-6h)
		−0.20	0.83		0.42	4.1% (AFM-2a)
	300 K	−0.20	0.09	6.15	0.40	56.50% (AFM-6h)
		−0.19	0.28		0.35	43.50% (AFM-2a)
	400 K	−0.33	0.36		0.42	100% (PM)

[a]Experimental uncertainties: isomer shift: I.S. ± 0.03 mm s^{-1}; quadrupole splitting: Q.S. ± 0.03 mm s^{-1}; line width: Γ ± 0.05 mm s^{-1}; hyperfine field: ±0.2 T; spectral contribution: ± 3%.

To determine the magnetic entropy change, a series of $M-T$ curves are measured for the Fe1.95 and Fe2.00 alloys, as shown in Figure 2c,f. A double peak is observed in the dM/dT curves for the Fe1.95 alloy, as shown in Figure S3a in the Supporting Information. Consequently, a double peak of magnetic entropy change is displayed in Figure 2e for the Fe1.95 alloy. The magnetic entropy change $|\Delta S_M|$ illustrated in Figure 2e,f is calculated from the isofield magnetization curves in Figure 2c,d based on the Maxwell relation: $\Delta S_M(\Delta H, T) = \int_{H_0}^{H} (\frac{\partial M(T,H)}{\partial T})_H \mathrm{d}\mu_0 H$, where we choose $\mu_0 H_0$ = 0 T. The maximal $|\Delta S_M|$ for the Fe1.95 alloy is 0.50 J/kg K at 170 K with a second peak value of 0.32 J/kg K at 237 K at a magnetic field change of 2 T. For the Fe2.00 alloy, its maximal $|\Delta S_M|$ is 0.39 J/kg K at 260 K at a magnetic field change of 2 T. The larger magnetization of the Fe1.95 alloy primarily contributes to its 22% larger magnetic entropy change compared to the Fe2.00 alloy. The maximal $|\Delta S_M|$ of the Fe1.95 alloy is comparable to other Fe-based Laves compounds with a second-order transition, with 0.5 J/kg K in $Sc_{0.4}Ti_{0.6}Fe_2$,[32] with 0.46 J/kg K in $Fe_2Hf_{0.85}Ti_{0.15}$[12] and with 1.3 J/kg K in rare-earth-free $Mn_{30}Fe_{20}Al_{50}$.[33] It is however smaller than the Fe-based Laves phase materials with a first-order transition, with 1.7 J/kg K in $Sc_{0.3}Ti_{0.7}Fe_2$[32] and 2.3 J/kg K in $Fe_2Hf_{0.86}Ta_{0.14}$.[8] For the latter, their saturation magnet-

https://doi.org/10.1021/acs.chemmater.4c01345
Chem. Mater. 2024, 36, 6299−6305

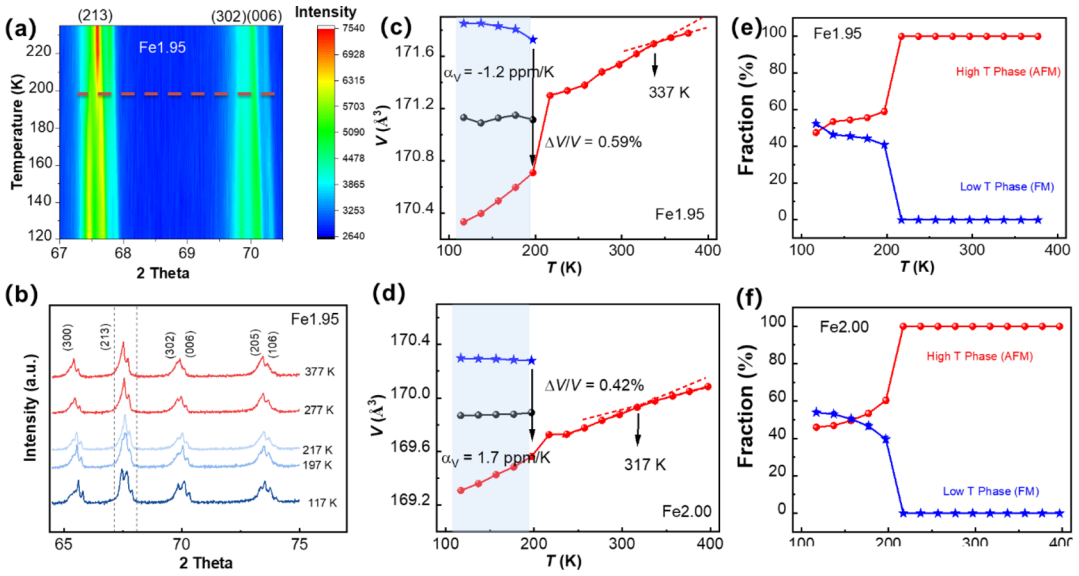

Figure 4. (a) Variable XRD intensity contour map showing the evolution of the Bragg peaks across the first-order magnetic transition. (b) XRD powder diffraction patterns, recorded upon heating at selected temperatures for the Fe1.95 alloy. Temperature dependence of the unit-cell volume for (c) Fe1.95 alloy and (d) Fe2.00 alloy. The blue shaded area indicates the coexistence of high-temperature and low-temperature ordered phases. The middle circle in the shaded area is the average unit-cell volume calculated from $V_{ave} = f_h \times V_h + f_l \times V_l$. The fraction evolution of the low- and high-temperature ordered phase for (e) Fe1.95 alloy and (f) Fe2.00 alloy.

izations are ~2.45 and 2.86 μ_B/f.u., respectively, larger than the value of 1.86 μ_B/f.u. for the Fe1.95 alloy. Therefore, the relatively small magnetic entropy change in Fe_2(Hf,Nb) results from the broad magnetic phase transition and suppressed saturation magnetization due to magnetic phase separation.

Figure 3 displays the Mössbauer spectra that were measured for the Fe1.95 alloy at temperatures of 4.2, 300, and 400 K. The fitting of the spectra is based on the crystal structure analysis, where Fe occupies two distinct sites, the 2a and 6h sites, with an atom ratio of 1:3. The spectrum at 400 K confirms the PM state at a high temperature. At room temperature, the sample exhibits an AFM state, affirming the complete transformation of the low-temperature ordered phase into the high-temperature ordered phase at 300 K. At 4.2 K, a coexistence of AFM and FM phases is observed, consistent with the $M-H$ curves. Table 1 summarizes the parameters fitted to the Mössbauer spectra at different temperatures. The isomer shifts for both the AFM and FM phases remain similar, implying an identical Fe valence state. However, the quadrupole splitting of Fe at the 2a site for the AFM phase significantly exceeds that of Fe at the 2a site for the FM phase This discrepancy indicates pronounced chemical environment distortions around Fe at the 2a site upon the transformation of the FM phase into the AFM phase with increasing temperature.[34] For the FM phase, the hyperfine field of Fe at the 6h site (18.0 T) and 2a site (14.1 T) is akin to the values observed in $Fe_2Hf_{0.83}Ta_{0.17}$ (19.0 and 13.6 T, respectively).[19] Conversely, for the AFM phase at 4.2 K, the hyperfine field of Fe at the 6h site (14.1 T) nearly doubles that observed at the 2a site (6.15 T) at 300 K. The fraction of the AFM phase at 4.2 K is approximately 20%, lower than the 48% of the high-temperature ordered phase at 117 K, as determined by variable-temperature XRD in Figure 4e. This indicates a gradual increase of the AFM phase with the rising temperature.

To investigate the evolution of the phases across the FM−AFM transition, powder XRD measurements were conducted for the Fe1.95 and Fe2.00 alloys over the temperature range of 117−397 K, as shown in Figures 4 and S4 in the Supporting Information. The crystal structures refined from the XRD diffraction patterns reveal that both alloys maintain the C14 hexagonal structure throughout the entire temperature range (with both Kα_1 and Kα_2 components present for each reflection). Focusing on the Fe1.95 alloy, upon cooling, the (213) peak splits into two peaks starting from 197 K, indicating the conversion of high-temperature ordered phase (AFM state) into the low-temperature ordered phase (FM state) with both phases coexisting as the temperature decreases until 117 K. These two magnetic phases share the same C14 crystal structure but possess slightly different lattice parameters. A similar magnetic phase separation phenomenon has been reported in $Fe_2Hf_{0.85}Nb_{0.15}$[23] and $Fe_2Ti_{0.70}Sc_{0.30}$[32] alloys with a coexistence of AFM and FM phases at low temperatures. It is noteworthy that the phase separation in Fe1.95 and Fe2.00 differs from the phase segregation reported in $Fe_2Hf_{0.6}Ti_{0.40}$, where Ti-rich and Ti-poor phases are observed at room temperature via SEM images.[12] The phase segregation in $Fe_2Hf_{0.60}Ti_{0.40}$ is suppressed by the rapid solidification process, but this method is ineffective for the magnetic phase separation in the $Fe_{1.95}$ alloy, as indicated by the similarly broad $M-T$ curves shown in Figure S5 in the Supporting Information. Compared to the Fe1.95 alloy, the peak splitting in the Fe2.00 alloy is less significant, indicating a weaker magnetic phase separation, as depicted in Supplementary Figure S4a. The volume change for the Fe1.95 alloy is 0.59% at 217 K, larger than the 0.42% change of the Fe2.00 alloy, as shown in Figure 4d. The critical temperature for a significant volume change is in agreement with T_t derived from the $M-T$ curve, confirming the nature of the magnetoelastic FM−AFM transition in $Fe_2Hf_{0.80}Nb_{0.20}$ alloys. A small kink at 337 K is attributed to the AFM−PM transition for the Fe1.95 alloy, which aligns with the kink at 340 K, as observed from the $M-T$ curve in the inset of Figure 2a.

Figure 4e,f shows the evolution of the phase fraction with temperature derived from variable-temperature XRD results.

https://doi.org/10.1021/acs.chemmater.4c01345
Chem. Mater. 2024, 36, 6299−6305

As the temperature increases, the fraction of the AFM phase for the Fe1.95 alloy increases from 48 to 60% and finally to 100%, indicating that the FM phase completely transformed into the AFM phase above 217 K. The Fe2.00 alloy shows a similar trend for the temperature evolution of the phase fractions. The XRD result, linear scanning of SEM image, and Mössbauer spectrum confirm the single-phase behavior of the Fe1.95 alloy; thus, this magnetic phase separation can be attributed to Fe vacancies introduced into the Fe1.95 alloy, as reported in the vacancy-induced phase separation in $La_{0.70}Ca_{0.30}Mn_{0.92}Cr_{0.08}O_z$[35] and Fe−Cr-based alloys.[36] The inhomogeneous distribution of Fe vacancies disrupts the movement of phase boundaries during the FM−AFM transition, thus inducing a two-step magnetization change, as shown in the $M-T$ curve of the Fe1.95 alloy.[34] The Fe2.00 alloy exhibits a relatively weak magnetic phase separation, leading to a singular broad $M-T$ curve and a correspondingly broad magnetic entropy change.

To explore the thermal expansion effect of $Fe_2Hf_{0.80}Nb_{0.20}$ alloys, the average unit-cell volume below 217 K is present within the blue shaded area in Figure 4c,d. The average volume is calculated from the formula $V_{ave} = f_h \times V_h + f_l \times V_l$, where f_h and f_l represent the fraction of the high-temperature and low-temperature ordered phase, and V_l and V_h the unit-cell volumes of both phases.[2] The volumetric coefficient of thermal expansion (α_V) for the Fe1.95 alloy is −1.2 ppm/K at the temperature range 117−197 K, which is smaller than the value for the Fe2.00 alloy (1.7 ppm/K). Both coefficients, in absolute terms, are below 3 ppm/K, categorizing the Fe1.95 and Fe2.00 alloys as ZTE materials. The value of α_V for the Fe1.95 alloy with a temperature span of 80 K is superior to most magnetic ZTE materials, such as $Fe_2Hf_{0.85}Ta_{0.15}C_{0.01}$[18] (2.4 ppm/K), $Mn_3Zn_{0.93}N$ (1.8 ppm/K),[26] $Fe_2Zr_{0.8}Nb_{0.2}$ (4.2 ppm/K),[37] $TbCo_{1.9}Fe_{0.1}$ (1.44 ppm/K),[38] and $Fe_{2.5}Hf_{0.80}Nb_{0.20}$ (3.21 ppm/K).[24] The $|\alpha_V|$ value of 1.2 ppm/K is also smaller than that of typical Invar alloys (4.5−7.5 ppm/K).[39] Such a pronounced ZTE in Fe_2(Hf,Nb) alloys originates from the competition between the positive thermal expansion of the AFM phase and the negative thermal expansion of the FM phase. DFT calculations by Yibole et al.[2] predict a tendency toward phase separation for Fe_2(Hf,Nb) alloys as an intrinsic property due to positive mixing energies. Introducing Fe vacancies regulates the competition between the AFM phase and the FM phase in terms of the unit-cell volume change or fraction evolution, and thus an enhanced ZTE is observed in the Fe1.95 alloy. The value of α_V decreases from a positive (1.7 ppm/K) to a negative (−1.2 ppm/K) value by inducing some Fe vacancies, which suggests that a more superior ZTE is feasible by further optimizing the concentration of Fe vacancies in Fe_2(Hf,Nb) alloys.[40]

CONCLUSIONS

Variable-temperature X-ray diffraction reveals two C14 hexagonal phases in the Fe1.95 and Fe2.00 alloys in a temperature range of 197−117 K. This observation is corroborated by Mössbauer spectra, confirming the coexistence of antiferromagnetic and ferromagnetic phases at 4.2 K. Notably, a two-step magnetic transition is evident in the Fe1.95 alloy, which demonstrates a larger magnetic entropy change of 0.5 J/kg K compared to 0.4 J/kg K in the Fe2.00 alloy, under a magnetic field change of 2 T. Additionally, a ZTE coefficient of −1.2 ppm/K is obtained in the Fe1.95 alloy, contrasting with the 1.7 ppm/K observed in the Fe2.00 alloy. The improved ZTE performance and enhanced magnetic entropy change achieved by the introduction of Fe vacancies hold promise as a new strategy to modulate the multifunctional applications in Fe-based Laves phase alloys.

ASSOCIATED CONTENT

Supporting Information

The Supporting Information is available free of charge at https://pubs.acs.org/doi/10.1021/acs.chemmater.4c01345.

Magnetic properties of the Fe1.95 and the Fe2.00 alloys; variable-temperature XRD of the Fe2.00 alloy; and magnetic properties of the melt-spun Fe1.95 alloy (PDF)

AUTHOR INFORMATION

Corresponding Author

Lingwei Li − *Key Laboratory of Novel Materials for Sensor of Zhejiang Province, Hangzhou Dianzi University, Hangzhou 310012, P.R. China;* orcid.org/0000-0001-8174-5351; Email: lingwei@hdu.edu.cn

Authors

Qi Shen − *Key Laboratory of Novel Materials for Sensor of Zhejiang Province, Hangzhou Dianzi University, Hangzhou 310012, P.R. China; Fundamental Aspects of Materials and Energy, Faculty of Applied Sciences, Delft University of Technology, Delft 2629 JB, The Netherlands;* orcid.org/0000-0002-0797-0312

Zeyu Zhang − *Key Laboratory of Novel Materials for Sensor of Zhejiang Province, Hangzhou Dianzi University, Hangzhou 310012, P.R. China*

Calvin de Vries − *Fundamental Aspects of Materials and Energy, Faculty of Applied Sciences, Delft University of Technology, Delft 2629 JB, The Netherlands;* orcid.org/0009-0003-0524-6106

Achim Iulian Dugulan − *Fundamental Aspects of Materials and Energy, Faculty of Applied Sciences, Delft University of Technology, Delft 2629 JB, The Netherlands*

Niels van Dijk − *Fundamental Aspects of Materials and Energy, Faculty of Applied Sciences, Delft University of Technology, Delft 2629 JB, The Netherlands*

Ekkes Brück − *Fundamental Aspects of Materials and Energy, Faculty of Applied Sciences, Delft University of Technology, Delft 2629 JB, The Netherlands*

Complete contact information is available at: https://pubs.acs.org/10.1021/acs.chemmater.4c01345

Notes

The authors declare no competing financial interest.

ACKNOWLEDGMENTS

This work was financially supported by Dutch Research Council (Grant No. 680-91-013) and Natural Science Foundation of China (Grant No. 52171174). Q.S. thanks Anton Lefering Bert Zwart and Robert Dankelman for their technical assistance.

REFERENCES

(1) Stein, F.; Leineweber, A. Review of their functional and structural applications and an improved fundamental understanding of stability and properties. *J. Mater. Sci.* **2021**, *56*, 5321−5427.

(2) Yibole, H.; Pathak, A. K.; Mudryk, Y.; Guillou, F.; Zarkevich, N.; Gupta, S.; Balema, V.; Pecharsky, V. K. Manipulating the stability of crystallographic and magnetic sub-lattices: A first-order magnetoelastic transformation in transition metal based Laves phase. *Acta Mater.* **2018**, *154*, 365−374.
(3) Song, Y.; Shi, N.; Deng, S.; Xing, X.; Chen, J. Negative thermal expansion in magnetic materials. *Prog. Mater. Sci.* **2021**, *121*, No. 100835.
(4) Nishihara, Y.; Yamaguchi, Y. Magnetic phase transitions in itinerant electron magnets $Hf_{1-x}Ta_xFe_2$. *J. Phys. Soc. Jpn.* **1983**, *52*, 3630−3636.
(5) Song, Y.; Sun, Q.; Xu, M.; Zhang, J.; Hao, Y.; Qiao, Y.; Zhang, S.; Huang, Q.; Xing, X.; Chen, J. Negative thermal expansion in $(Sc,Ti)Fe_2$ induced by an unconventional magnetovolume effect. *Mater. Horiz.* **2020**, *7*, 275−281.
(6) Li, B.; Luo, X. H.; Wang, H.; Ren, W. J.; Yano, S.; Wang, C. W.; Gardner, J. S.; Liss, K. D.; Miao, P.; Lee, S. H.; Kamiyama, T.; Wu, R. Q.; Kawakita, Y.; Zhang, Z. D. Colossal negative thermal expansion induced by magnetic phase competition on frustrated lattices in Laves phase compound $(Hf,Ta)Fe_2$. *Phys. Rev. B* **2016**, *93*, No. 224405.
(7) Li, L. F.; Tong, P.; Zou, Y. M.; Tong, W.; Jiang, W. B.; Jiang, Y.; Zhang, X. K.; Lin, J. C.; Wang, M.; Yang, C.; Zhu, X. B.; Song, W. H.; Sun, Y. P. Good comprehensive performance of Laves phase $Hf_{1-x}Ta_xFe_2$ as negative thermal expansion materials. *Acta Mater.* **2018**, *161*, 258−265.
(8) Diop, L. V. B.; Isnard, O.; Amara, M.; Gay, F.; Itié, J. P. Giant negative thermal expansion across the first-order magnetoelastic transition in $Hf_{0.86}Ta_{0.14}Fe_2$. *J. Alloys Compd.* **2020**, *845*, No. 156310.
(9) Moriya, T.; Usami, K. Coexistence of ferro- and antiferromagnetism and phase transitions in itinerant electron systems. *Solid State Commun.* **1977**, *23*, 935−938.
(10) Rechenberg, H. R.; Morellon, L.; Algarabel, P. A.; Ibarra, M. R. Magnetic moment at highly frustrated sites of antiferromagnetic Laves phase structures. *Phys. Rev. B* **2005**, *71*, No. 104412.
(11) Diop, L. V. B.; Isnard, O.; Suard, E.; Benea, D. Neutron diffraction study of the itinerant-electron metamagnetic $Hf_{0.825}Ta_{0.175}Fe_2$ compound. *Solid State Commun.* **2016**, *229*, 16−21.
(12) Shen, Q.; Batashev, I.; Zhang, F.; Ojiyed, H.; Dugulan, I.; van Dijk, N.; Brück, E. Exploring the negative thermal expansion and magnetocaloric effect in $Fe_2(Hf,Ti)$ Laves phase materials. *Acta Mater.* **2023**, *257*, No. 119149.
(13) Diop, L. V. B.; Benea, D.; Mankovsky, S.; Isnard, O. Cross over between ferro and antiferromagnetic order in Fe itinerant electron magnetism: An experimental and theoretical study of the model $(Hf,Ta)Fe_2$ Laves phases. *J. Alloys Compd.* **2015**, *643*, 239−246.
(14) Duijn, H. G. M.; Brück, E.; Menovsky, A. A.; Buschow, K. H. J.; de Boer, F. R.; Coehoorn, R.; Winkelmann, M.; Siemensmeyer, K. Magnetic and transport properties of the itinerant electron system $Hf_{1-x}Ta_xFe_2$. *J. Appl. Phys.* **1997**, *81*, 4218−4220.
(15) Diop, L. V. B.; Kastil, J.; Isnard, O.; Arnold, Z.; Kamarad, J. Magnetic and magnetocaloric properties of itinerant-electron system $Hf_{1-x}Ta_xFe_2$ (x = 0.125 and 0.175). *J. Alloys Compd.* **2015**, *627*, 446−450.
(16) Song, Z.; Li, Z.; Yang, B.; Yan, H.; Esling, C.; Zhao, X.; Zuo, L. Large Low-Field Reversible Magnetocaloric Effect in Itinerant-Electron $Hf_{1-x}Ta_xFe_2$ Alloys. *Materials* **2021**, *14*, 5233 DOI: 10.3390/ma14185233.
(17) Huang, S.; Wang, D.; Han, Z.; Su, Z.; Tang, S.; Du, Y. Magnetic and magnetocaloric properties of quenched $Hf_{1-x}Ta_xFe_2$ materials. *J. Alloys Compd.* **2005**, *394*, 80−82.
(18) Xu, J.; Wang, Z.; Huang, H.; Li, Z.; Chi, X.; Wang, D.; Zhang, J.; Zheng, X.; Shen, J.; Zhou, W.; Gao, Y.; Cai, J.; Zhao, T.; Wang, S.; Zhang, Y.; Shen, B. Significant Zero Thermal Expansion Via Enhanced Magnetoelastic Coupling in Kagome Magnets. *Adv. Mater.* **2023**, *35*, No. 2208635.
(19) Shen, Q.; Zhang, F.; Dugulan, I.; van Dijk, N.; Brück, E. Magnetoelastic transition and negative thermal expansion of $Fe_2Hf_{0.83}Ta_{0.17}$ ribbons. *Scr. Mater.* **2023**, *232*, No. 115482.
(20) Cen, D.; Wang, B.; Chu, R.; Gong, Y.; Xu, G.; Chen, F.; Xu, F. Design of $(Hf,Ta)Fe_2/Fe$ composite with zero thermal expansion covering room temperature. *Scr. Mater.* **2020**, *186*, 331−335.
(21) Fujita, A.; Fujieda, S.; Hasegawa, Y.; Fukamichi, K. Itinerant-electron metamagnetic transition and large magnetocaloric effects in $La(Fe_xSi_{1-x})_{13}$ compounds and their hydrides. *Phys. Rev. B* **2003**, *67*, No. 104416.
(22) Dung, N. H.; Ou, Z. Q.; Caron, L.; Zhang, L.; Thanh, D. T. C.; de Wijs, G. A.; de Groot, R. A.; Buschow, K. H. J.; Brück, E. Mixed magnetism for refrigeration and energy conversion. *Adv. Energy Mater.* **2011**, *1*, 1215−1219.
(23) Song, Y.; Chen, J.; Liu, X.; Wang, C.; Gao, Q.; Li, Q.; Hu, L.; Zhang, J.; Zhang, S.; Xing, X. Structure, Magnetism, and Tunable Negative Thermal Expansion in $(Hf,Nb)Fe_2$ Alloys. *Chem. Mater.* **2017**, *29*, 7078−7082.
(24) Dong, X.; Lin, K.; Yu, C.; Zhang, W.; Li, W.; Zhang, Q.; Zhang, Q.; Liu, J.; Cao, Y.; Xing, X. Zero thermal expansion in non-stoichiometric and single-phase $(Hf,Nb)Fe_{2.5}$ alloy. *Scr. Mater.* **2023**, *229*, No. 115388.
(25) Xu, M.; Song, Y.; Xu, Y.; Sun, Q.; Long, F.; Shi, N.; Qiao, Y.; Zhou, C.; Ren, Y.; Chen, J. High-Temperature Zero Thermal Expansion in $HfFe_{2+\delta}$ from Added Ferromagnetic Paths. *Chem. Mater.* **2022**, *34*, 9437−9445.
(26) Wang, C.; Chu, L.; Yao, Q.; Sun, Y.; Wu, M.; Ding, L.; Yan, J.; Na, Y.; Tang, W.; Li, G.; Huang, Q.; Lynn, J. W. Tuning the range, magnitude, and sign of the thermal expansion in intermetallic $Mn_3(Zn,M)_xN$ (M = Ag, Ge). *Phys. Rev. B* **2012**, *85*, No. 220103.
(27) Toby, B. H. R factors in Rietveld analysis: How good is good enough? *Powder Diffr.* **2006**, *21*, 67−70.
(28) Klencsar, Z. Mössbauer spectrum analysis by evolution algorithm. *Nucl. Instrum. Meth. B* **1997**, *129*, 527−533.
(29) Herbst, J. F.; Fuerst, C. D.; McMichael, R. D. Structural, magnetic, and magnetocaloric properties of $(Hf_{0.83}Ta_{0.17})Fe_{2+x}$ materials. *J. Appl. Phys.* **1996**, *79*, 5998.
(30) Wada, H.; Shimamura, N.; Shiga, M. Thermal and transport properties of $Hf_{1-x}Ta_xFe_2$. *Phys. Rev. B* **1993**, *48*, 10221−10226.
(31) Raghavendra Reddy, V.; Rawat, R.; Gupta, A.; Bag, P.; Siruguri, V.; Chaddah, P. Low temperature high magnetic field ^{57}Fe Mössbauer study of kinetic arrest in Ta doped $HfFe_2$. *J. Phys. Condens.* **2013**, *25*, No. 316005.
(32) Song, Y.; Xu, M.; Zheng, X.; Zhou, C.; Shi, N.; Huang, Q.; Wang, S.; Jiang, Y.; Xing, X.; Chen, J. A new method to enhance the magnetocaloric effect in $(Sc,Ti)Fe_2$ via magnetic phase separation. *J. Mater. Sci. Technol.* **2023**, *147*, 102−111.
(33) Zhang, Y.; Hao, W.; Hu, C.; Wang, X.; Zhang, X.; Li, L. Rare-Earth-Free $Mn_{30}Fe_{20-x}Cu_xAl_{50}$ Magnetocaloric Materials with Stable Cubic CsCl-Type Structure for Room-Temperature Refrigeration. *Adv. Funct. Mater.* **2023**, *33*, No. 2310047.
(34) Huang, D.; Ma, T.; Brown, D. E.; Lapidus, S. H.; Ren, Y.; Gao, J. Nanoscale Phase Separation and Large Refrigerant Capacity in Magnetocaloric Material $LaFe_{11.5}Si_{1.5}$. *Chem. Mater.* **2021**, *33*, 2837−2846.
(35) Tian, J. J.; Fang, J.; Chen, J. L.; Zhang, W. F. The influence of deoxygenation on the magnetic and electrical properties of $La_{0.70}Ca_{0.30}Mn_{0.92}Cr_{0.08}O_z$ ($2.897 \leq z \leq 2.998$). *Phys. Lett. A* **2007**, *363*, 307−311.
(36) Yan, Z.; Shi, S.; Li, Y.; Chen, J.; Maqbool, S. Vacancy and interstitial atom evolution with the separation of the nanoscale phase in Fe−Cr alloys: phase-field simulations. *Phys. Chem. Chem. Phys.* **2020**, *22*, 3611−3619.
(37) Song, Y.; Sun, Q.; Yokoyama, T.; Zhu, H.; Li, Q.; Huang, R.; Ren, Y.; Huang, Q.; Xing, X.; Chen, J. Transforming Thermal Expansion from Positive to Negative: The Case of Cubic Magnetic Compounds of $(Zr,Nb)Fe_2$. *J. Phys. Chem. Lett.* **2020**, *11*, 1954−1961.
(38) Song, Y.; Chen, J.; Liu, X.; Wang, C.; Zhang, J.; Liu, H.; Zhu, H.; Hu, L.; Lin, K.; Zhang, S.; Xing, X. Zero Thermal Expansion in Magnetic and Metallic $Tb(Co,Fe)_2$ Intermetallic Compounds. *J. Am. Chem. Soc.* **2018**, *140*, 602−605.

(39) van Schilfgaarde, M.; Abrikosov, I. A.; Johansson, B. Origin of the Invar effect in iron-nickel alloys. *Nature* **1999**, *400*, 46−49.
(40) Xie, L.; Lin, J.; Zhong, X.; Dong, B.; Wang, R.; Zhu, X.; Tong, P.; Song, W.; Sun, Y. Zero thermal expansion, high specific thermal conductivity, and good machinability of $Cu_2P_2O_7$/2024Al composite. *Ceram. Int.* **2023**, *49*, 35617−35622.

https://doi.org/10.1021/acs.chemmater.4c01345
Chem. Mater. 2024, 36, 6299−6305